Energy Transfer Strategy for Urban Rail Transit Battery Energy Storage System to Reduce Peak Power of Traction Substation

Qiangqiang Qin, *Student Member, IEEE*, Tingting Guo, *Student Member, IEEE*, Fei Lin, *Member, IEEE*, and Zhongping Yang, *Member, IEEE*

***Abstract*—In order to reduce the peak power of traction substation as much as possible and make better use of the configuration capacity of battery energy storage system (BESS) in urban rail transit, a BESS control strategy based on energy transfer is proposed. Based on the actual subway line data, the load characteristics of urban rail transit with different departure intervals are analyzed by using the simulation platform of urban rail transit traction power supply system. Then, based on the characteristics of urban rail traffic load and the high energy density of the battery, the SOC dynamic adjustment module and discharge threshold dynamic adjustment module were added. The discharge threshold is dynamically adjusted according to the SOC of the battery, and part of regenerative braking energy absorbed by the energy storage device is transferred from off-peak/flat peak period to peak period for release. The simulation model and 90 kW physical platform are used to verify the proposed control strategy, and the results show that the control strategy can effectively realize energy transfer. Not only can achieve energy saving and voltage stability, but also can effectively reduce the peak power of traction substation, bring more economic benefits.**

***Index Terms*—Battery energy storage system, dynamic threshold, energy management strategy, energy transfer, urban rail transit.**

I. Introduction

DUE to the short distance between urban rail transit stations and frequent train braking, considerable regenerative braking energy is generated during braking. However, the modern urban rail transit traction substation adopts the diode uncontrolled rectification mode. The train's regenerative braking energy cannot be returned to the AC grid through the traction substation, and the residual regenerative braking energy will cause the DC grid voltage to rise and suppress the train regenerative braking. The application of energy storage systems(ESS) to recover the remaining regenerative braking energy has become the current research hotspot [1]–[3]. Supercapacitors (SCs), batteries, flywheels and other ESS have many applications in urban rail transit. Among them, the lithium-ion battery technology has developed rapidly, and its capacity level and power level can meet the regenerative braking energy absorption and release requirements of rail transit. At present, the BESS has been practically applied in urban rail transit. At the same time, the SC is also used in the energy absorption of regenerative braking of rail transit with virtue of its high power and long cycle life [4]–[21].

In order to better achieve the battery energy storage effect, researchers are conducting in-depth research on battery control strategies. Reference [11] adopts a fixed charging and discharging threshold strategy. In order to prevent the battery from overcharging or over discharging due to multiple charge and discharge imbalances, a small current charge/discharge is performed during standby of the energy storage system, adjusting battery SOC (State of charge) [12] to maintain it near a certain value. However, this unnecessary charging and discharging will accelerate the degradation of the battery. Considering the battery life, reference [13] proposes a dynamic threshold strategy, which adjusts the discharge threshold of the energy storage system according to the SOC of the battery (V-SOC control), and controls the SOC within a certain range. By analyzing the battery's charging characteristics, Doshisha University proposed a control strategy of maximum power point tracking (I-SOC control), which adjusts the maximum discharge current of the battery according to the battery SOC, to maintain the battery SOC near the maximum power point. So that, in the same capacity configuration, the energy saving effect of the ESS can be increased [14]. However, there are relatively few studies considering the impact of the characteristics of the BESS. Different from power elements such as SC [15]–[22], lithium battery energy storage system can recover the remaining regenerative braking energy, and its high energy density makes it possible to provide traction energy for trains in long power supply intervals or high departure density, to improve the voltage drop of the network and reduce the capacity of traction substations [23].

Loads of rail trains are closely related to departure intervals. During the off-peak periods, the substation output power is low and the residual regenerative braking energy is high in the process of train operation, the peak period is opposite. However, the traction substation is mainly designed according to the peak

Manuscript received November 21, 2018; revised April 1, 2019, June 12, 2019, and August 5, 2019; accepted October 10, 2019. Date of publication October 21, 2019; date of current version December 17, 2019. This work was supported by the National Key R&D Program of China under Grant 2017YFB1201105 (2017–2020). The review of this article was coordinated by Prof. S. Manshadi. *(Corresponding author: Qiangqiang Qin.)*

Q. Qin, F. Lin, and Z. Yang are with the Beijing Jiaotong University, Beijing 100044, China (e-mail: 17121483@bjtu.edu.cn; flin@bjtu.edu.cn; zhpyang@bjtu.edu.cn).

T. Guo is with the Beijing Hyperstrong Technology Co., Ltd., Beijing 100000, China (e-mail: 15121410@bjtu.edu.cn).

Digital Object Identifier 10.1109/TVT.2019.2948766

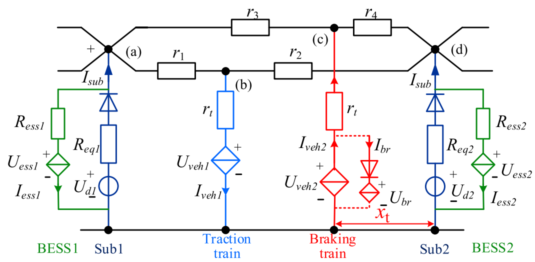

Fig. 1. Urban rail traction power supply model with ESS.

power during peak period. Therefore, if the characteristics of high energy density of batteries are utilized, part of regenerative braking energy in off-peak period is temporarily stored and transferred to peak period for release. It will effectively reduce the peak power of traction substation in peak period. So the operation cost of substation and the construction cost of new substation can be reduced.

Therefore, this paper puts forward a strategy of energy transfer for BESS based on SOC tracking (T-SOC) at different departure intervals to reduce the peak power of the traction substation. In the second part, a simulation model of urban rail traction power supply is built and the energy flow characteristics of urban rail DC traction network are analyzed. The third part analyses the impact of energy storage systems on the output of substations. The fourth part puts forward T-SOC strategy of energy shifting for BESS based on SOC tracking at different period. In the fifth part, through the simulation of an actual line, the validity and rationality of the adjustment methods are verified. Experimental results and discussions are given in Section VI. In Section VII, the summary is given.

II. Urban Rail Transit DC Power Supply Network Energy Analysis and Mathematical Model

In order to analyze the energy flow characteristics of urban rail transit, this paper builds a simulation model of urban rail power supply system including energy storage device. The urban rail transit DC traction power supply network structure is shown in Fig. 1 [24]. It includes traction substations, trains and wayside BESS. The upline and downline trains run at the same time. The line impedance r_i between the train and the substation is time-varying, and its value will change in real time with the change of train position [25]. r_t is the quivalent series resistance of train.

A. Traction Substation

The traction substation equivalent model consists of an ideal voltage source U_d, an equivalent internal resistance R_{eq} and a diode. In actual operation, the output of the substation is nonlinear [26]. As shown in Fig. 2, the piecewise linearization process method is used. The output voltage U_{sub} is shown in Equation (1). U_{d0} is the no-load voltage of the substation. When $I_{\text{sub}} \le I_g$, $U_d = U_{d0}$, $R_{eq} = R_{eq1}$; when $I_{\text{sub}} > I_g$, $U_d = U_{d1}$, $R_{eq} = R_{eq2}$. I_{sub} is the output current of the substation, I_g is the critical current [27], [28].

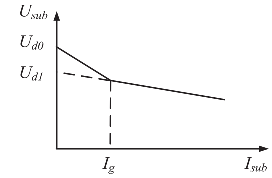

Fig. 2. Output characteristics of twelve-pulse rectifier.

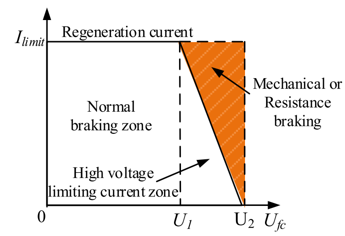

Fig. 3. Train current limiting characteristics.

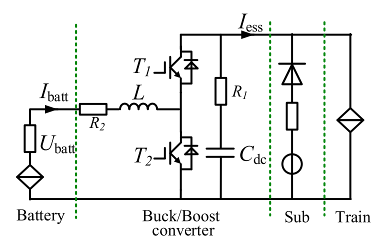

Fig. 4. BESS structure.

$$U_{\text{sub}} = \begin{cases} U_{\{d}0 - I_{\text{sub}} * R_{eq1}; & I_{\text{sub}} \le I_g \\ U_{d1} - I_{\text{sub}} * R_{eq2}; & I_{\text{sub}} > I_g \end{cases} \tag{1}$$

B. Train

The train is equivalent to the controlled current sources I_{veh} and $I_{\text{veh\_up}}$, in order to simulate the traction current absorbed by the train from the DC power supply network and feedback braking current. In addition, considering the current limiting characteristics of the train in braking [29], when the train pantograph voltage U_t is greater than U_1, the train regenerative current begins to be limited; when U_t is greater than U_2, the train regenerative braking fails, as shown in Fig. 3. U_{fc} is the pantograph voltage of train, I_{limit} is the limit value of regenerative braking current of train. The train running current is shown in Equation (2).

$$I_{\text{veh}} = \begin{cases} P_t/U_t, & U_t < U_1 \\ \max\left[\frac{P_t}{U_t}, -I_{\max} * \left(\frac{U_t - U_2}{U_2 - U_1}\right)\right], & U_1 < U_t < U_2 \\ 0, & U_t > U_2 \end{cases} \tag{2}$$

where P_t—train operating power, $I_{\max}$—maximum current for train regenerative braking.

C. BESS and Control Pattern

The BESS consists of bidirectional DC/DC converters and battery packs, as shown in Fig. 4. Among bidirectional DC/DC

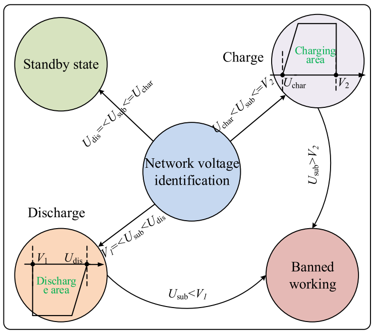

Fig. 5. BESS modal switching principle.

converters perform functions of system voltage level conversion and energy management [30].

where U_{batt}—battery voltage, I_{batt}—battery current, L— chopping inductor, C_{dc}—filter capacitor, R_1 and R_2—equivalent internal resistance respectively.

BESS adopts traditional double closed loop control: The outer ring is the bus voltage loop, the inner ring is the battery current loop [25]. The working state is determined by the bus voltage U_{sub}. The switching principle is shown in Fig. 5. U_{sub} is greater than the charging threshold U_{char}, the system enters the state of charge to recover the remaining regenerative braking energy; when U_{sub} is less than the discharge threshold U_{dis}, the system enters the discharge state to provide energy for the train; when U_{sub} is between the charge and discharge thresholds, the system is in standby mode; If U_{sub} is lower than the voltage lower limit value V_1 or higher than the voltage upper limit value V_2, the system is in a disabled operation state [9], [30].

The BESS has a voltage stabilizing effect, and it is essentially a controlled current source I_{ess} [31]. R_{ess} is the equivalent internal resistance of the battery and the DC/DC converter. When the power command $P_{\text{batt-ref}}$ is less than the rated power $P_{\text{batt-max}}$ of the ESS, the bus voltage is clamped to the voltage command value $U_{\text{dis}}/U_{\text{char}}$. Conversely, the voltage cannot be clamped, and the ESS is charged and discharged at the rated power, as shown in Equation (3).

$$\begin{cases} I_{\text{ess}} = P_{\text{batt-ref}}/U_{\text{sub}}, (P_{\text{batt-ref}} < P_{\text{batt-max}}) \\ I_{\text{ess}} = P_{\text{batt-max}}/U_{\text{sub}}, (P_{\text{batt-ref}} \geq P_{\text{batt-max}}) \\ U_{\text{sub}} = U_{\text{char}} \text{ or } U_{\text{dis}} \end{cases} \tag{3}$$

D. Urban Rail Energy Flow

The urban rail transit DC traction power supply network mainly includes traction substations, trains and wayside BESS. The energy flow of the traction power supply system is complexly shown in Fig. 6. The braking energy (E_b) of the train mainly has four flow paths, one part is provided to the adjacent traction train (E_{cross}), one part is lost on the line impedance (E_{line}), one part is stored in the BESS (E_c), and the rest part is consumed as heat (E_m) by mechanical braking or on-board braking resistors. The traction energy (E_t) of the train mainly comes from the traction substation (E_{sub}), the adjacent brake train (E_{cross}) and the BESS (E_d).

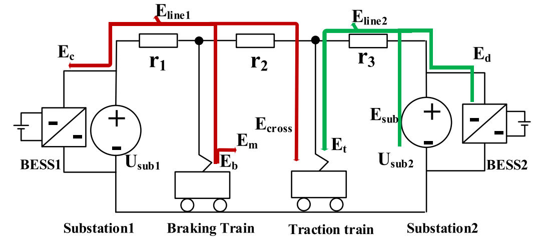

Fig. 6. Urban rail traffic energy flow diagram.

TABLE I
SUBSTATION PARAMETERS

Parameter	U_{d0}/V	U_{d1}/V	R_{eq1}/Ω	R_{eq2}/Ω	I_g/A
Value	836	784	0.07	0.0136	742.8

TABLE II
LINE PARAMETERS

Substation number	1	2	3	4	5
Position /km	0	1.93	4.08	6.39	8.51

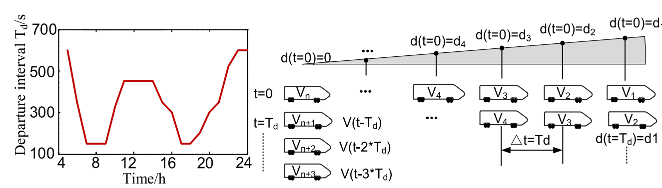

Fig. 7. Train departure interval and train distribution.

E. Urban Rail Transit Energy Flow Without BESS

In order to better analyze the characteristics of urban rail traffic load, based on the parameters of a certain line in Beijing Subway, this paper establishes a multi-train operating model with 5 substations. According to the measured data, the substation parameters and the line parameters are shown in Table I and Table II, respectively. The running time T of the train from the initial station to the terminal station is 889s, and the upline and downline trains are running simultaneously.

The train's departure interval T_d and distribution are shown in Fig. 7. The maximum departure interval is 600s, and the minimum departure interval is 150s. Take the above line as an example, there will be a train V_n senting out from the starting station at every departure interval T_d. When the number of trains running on the line reaches saturation, the number of trains running at the same time is $n = floor(T/T_d)$ or $ceil(T/T_d)$. Where *floor* is rounded down and *ceil* is rounded up. The distance between the trains is related to the train running curve. The power demand of all the trains on the line changes periodically with the different departure interval T_d.

The typical departure interval is selected for simulation. The situation energy flow on different departure interval from 150s to 600s (every 50s) is shown in Fig. 8. Among Fig. 8(a) shows the interaction energy at different departure intervals (which can be obtained from the total braking energy of the train and the energy consumed by mechanical braking). Fig. 8(b) shows the total traction energy consumption and substation output energy

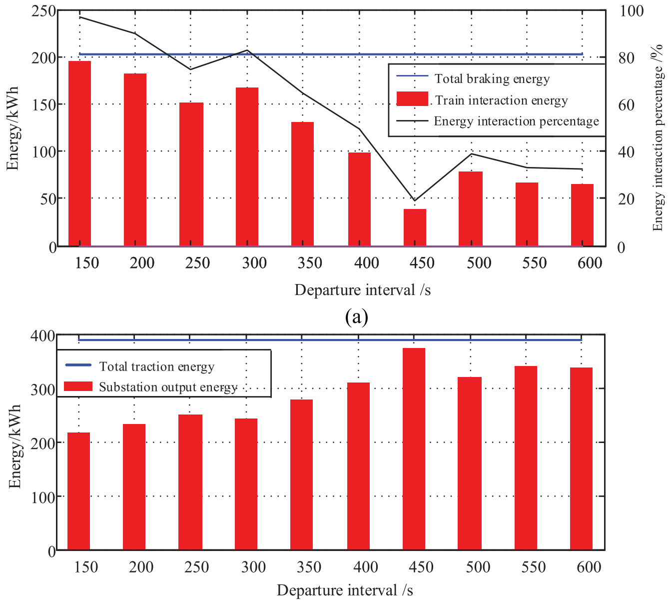

Fig. 8. Energy flow at different departure intervals. (a) Train interaction energy at different departure intervals. (b) The output energy of the substation at different departure intervals.

consumption at different departure intervals. From Fig. 8, it can be seen that the total train traction energy and the total braking energy are the same under different departure intervals. The reason is that the traction and braking energy of all trains in a departure interval can be equivalent to the traction and braking energy of a train running from the starting station to the terminal station. When the departure interval is 0~300s, the train density is very high throughout the line. The frequency of energy interaction plays a leading role, the energy interaction between trains is relatively high, the remaining braking energy is less, and the total train traction energy is certain, so the energy output of substations is less. As the departure interval increases, the frequency of energy interaction between trains decreases, so the energy output from substations tends to increase.

However, the output energy from substations per unit time is reduced. The output power of a substation at a typical departure interval is shown in Fig. 9. The average power and peak power of substation No. 3 at different departure intervals is shown in Fig. 10. The average power $P_{\text{ave}}(i)$ is the ratio of the energy $E_{\text{sub}}(i)$ output from the i-th substation to the departure interval in a single departure interval, as shown in Equation (4). It can be seen that as the departure interval increases, P_{ave} and the peak power P_{peak} tend to decrease and then remain basically constant. Because when the departure interval decreases, the number of trains running on the line at the same time increases, the power demand increases too, and the output power of the substation also rises. As the departure interval increases, the number of trains running on the line at the same time reduces. When the departure interval T_d is large enough, there is only one train in the power supply range of the substation, the peak power and average power of the substation approximate one-half of the average power and peak power of the single train (Substations

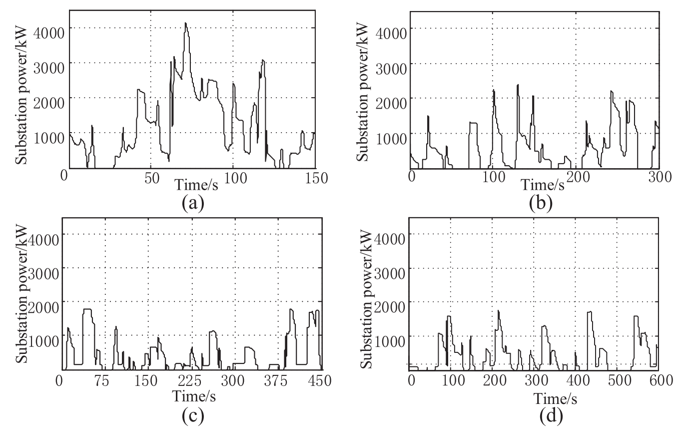

Fig. 9. The output power of the substation at different departure intervals. (a) $T_d = 150$ s. (b) $T_d = 300$ s. (c) $T_d = 450$ s. (d) $T_d = 600$ s.

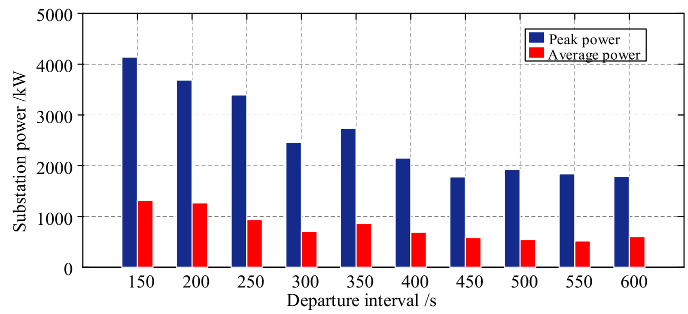

Fig. 10. The output power of the substation at different departure intervals.

are powered bilaterally).

$$P_{ave} = E_{\text{sub}}/T_d \tag{4}$$

The capacity of the traction substation is designed according to the peak power. However, it can be seen from Fig. 9 that the peak power of the train in the off-peak period is the largest, approximately 4000 kW. From Fig. 10, the peak power of the substation is much larger than the average power, and the relationship can be up to 4 times. The designed capacity of the traction substation according to peak power will be large, resulting in a large overall cost of the system. Therefore, when the departure interval is small enough, it is possible to reduce the peak power, then the configuration capacity of traction substation will also reduce the overall cost is reduced accordingly.

III. Urban Rail Transit Energy Flow With BESS

The 2 MW BESS is taken as an example to analyze the energy flow of the urban rail with the BESS, as shown in Fig. 11. The ESS adopts the traditional V-SOC control strategy, which adjusts the discharge threshold U_{dis} according to the SOC of the battery. Controls the discharge capacity of the ESS, realizes the charge and discharge energy balance, and prevents the battery from overcharging and overdischarging. From Fig. 11, it can be seen that as the departure interval increases, the energy recovered by the ESS tends to increase as the interaction energy of the train decreases, and the energy recovered by the ESS is released again when the train is in traction. So, the energy output from the

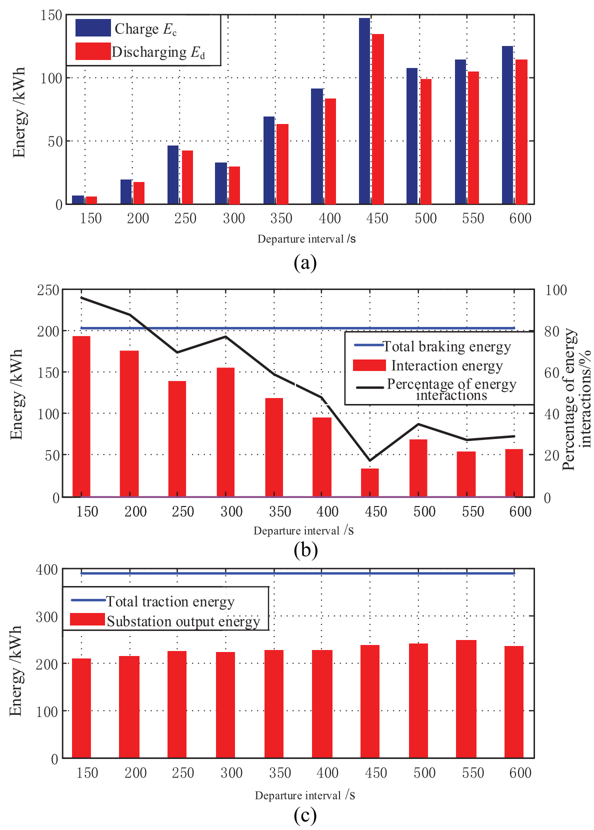

Fig. 11. Energy flow at different departure intervals. (a) ESS charge and discharge energy. (b) Train interaction energy. (c) Substation output energy.

substation is reduced, and the amount of reduction is related to the energy recovered by the ESS. Moreover, due to the internal resistance of the battery and the loss of the bidirectional DC/DC converter, the energy output from the BESS to the DC network is less than the charge capacity.

When the train operates in the tractive condition, the substation and the ESS provide traction energy at the same time. The working state of the ESS will affect the output of the substation. When the load power P_{load} is small, the output voltage of the substation is greater than the discharge threshold U_{dis}, the ESS does not work. As the load power increases, when the load power is greater than the calculated power value $P_{\text{thershold}}$ in Equation (5), the voltage of the substation drops to the discharge threshold U_{dis}, and the ESS begins to enter the discharge state. The discharge power of the ESS $P_{\text{batt-dis}}$ is shown in Equation (6). The ESS discharge E_d is shown in Equation (7). From Equations (5) to (7), it can be seen that under the same load, the larger discharge threshold is, the smaller corresponding power threshold is, and the larger discharge amount E_d of ESS is.

$$P_{\text{threshold}} = U_{\text{dis}} * U_d / R_{eq2} - U_{\text{dis}}^2 / R_{eq2} \tag{5}$$

$$P_{\text{batt-dis}} = \begin{cases} P_{\text{load}} - P_{\text{threshold}}, & (0 < P_{\text{load}} - P_{\text{threshold}} < P_{\text{batt\_max}}) \\ P_{\text{batt\_max}}, & (P_{\text{load}} - P_{\text{threshold}} \geq P_{\text{batt\_max}}) \end{cases} \tag{6}$$

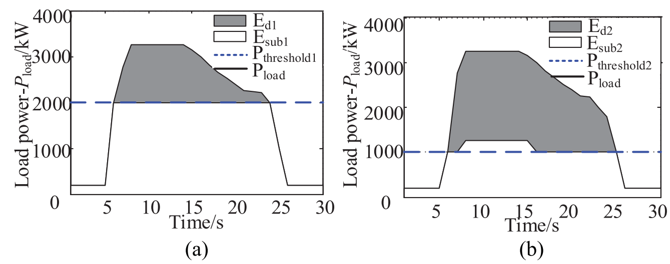

Fig. 12. Substation and ESS output. (a) $P_{\text{threshold1}} = 2000$ kW. (b) $P_{\text{threshold2}} = 1000$ kW.

$$E_d = \int P_{\text{batt-dis}} dt \tag{7}$$

Take simple traction as an example, assuming $P_{\text{batt\_max}}$ is 2000 kW, when U_{dis1} is 747.62 V and U_{dis2} is 766.25 V, the $P_{\text{threshold1}}$ is 2000 kW and $P_{\text{threshold2}}$ is 1000 kW. Fig. 12 shows the output power of the substation and the ESS under different discharge thresholds. The shaded part is the discharge power and discharge energy of the ESS, and the white part is the output power and energy of the substation. It can be seen from Fig. 12 that $E_{d1} < E_{d2}$, the value of $P_{\text{sub}}^{\text{peak,1}}$ is approximately 2000 kW, the value of $P_{\text{sub}}^{\text{peak,2}}$ is approximately 1400 kW, $P_{\text{sub}}^{\text{peak,1}} > P_{\text{sub}}^{\text{peak,2}}$. Can be obtained from the data results, if the discharge energy of the ESS can be increased, the peak power of the substation can be effectively reduced.

In V-SOC control strategies, discharge thresholds are dynamically adjusted based on battery SOC to maintain SOC within a certain range. The amount of discharge E_d of the ESS depends on the recovered energy E_c. It can be seen from Fig. 9 that the peak power of the substation is the largest at the off- peak period. Under the V-SOC control strategy, although the ESS can simultaneously reduce the peak power at different peaks, the peak power is reduced less during the peak period. The substation capacity reduction is not very obvious. Therefore, it is necessary to consider the new strategy to reduce the peak power at the peak period and significantly reduce the design capacity of the traction substation. Through the above analysis, we can see that during the peak period, the remaining regenerative braking energy is less, the peak power of the sub-station is larger, so the discharge amount of the ESS E_d is smaller. If the advantage of energy density of the BESS can be utilized to shift the regenerative braking energy recovered during the off-peak period/flat period to the peak period, the discharge energy E_d of the ESS during the peak period can be increased, and the peak power of substations can be decreased.

IV. Dynamic Adjustment Strategy for Discharge Threshold of BESS Based on Energy Transfer(T-SOC)

In order to achieve the transfer of energy from the off-peak period to the peak period, this paper adds the SOC_{ref} dynamic adjustment module based on the existing control strategy, so that the SOC of the battery is no longer confined to a certain range and changes with the departure interval. In the off-peak period, the battery SOC increases dynamically to increase the

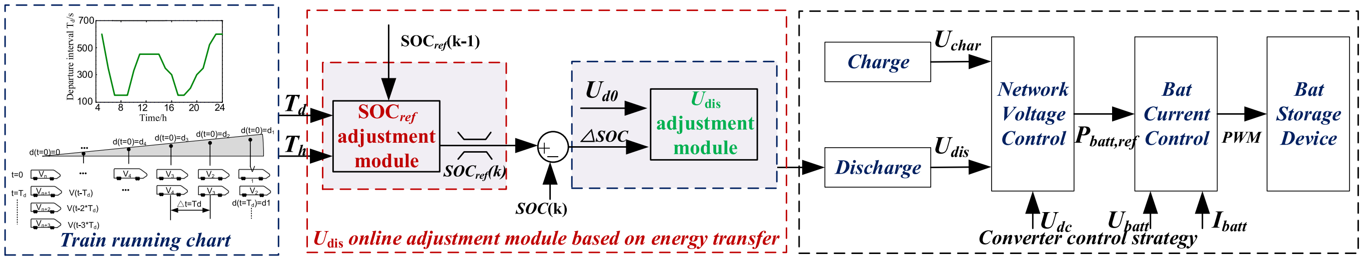

Fig. 13. Dynamic threshold strategy control block diagram of BESS based on energy transfer.

energy storage of ESS; In the peak period, the battery SOC decreases dynamically to release energy storage of the ESS. The charging threshold U_{char} will affect the regenerative braking energy E_c recovered by the ESS. The discharge threshold U_{dis} will affect the discharge amount E_d of the ESS. In order to ensure the effective absorption of the remaining regenerative braking energy, the charging threshold is set to a fixed value. This article only dynamically adjusts the discharge threshold.

As shown in Fig. 13, the control strategy is divided into two parts: SOC dynamic adjustment module and discharge threshold adjustment module.

A. SOC Dynamic Adjustment Module

This module mainly controls the energy transferred from the off-peak period to the peak period with SOC_{ref}. For actual urban rail line, the departure interval T_d of the train is determined in advance. The T_d and the remaining duration T_h of the current departure interval can be obtained in real time based on the communication, so SOC_{ref} can be determined according to the train departure interval and its remaining duration, as shown in Equation (8).

$$\text{SOC}_{\text{ref}}(k) = \text{SOC}_{\text{ref}}(k-1) + k_1 * \Delta t$$
$$k_1 = (\text{SOC}_{\text{ref}}^{\text{end}} - \text{SOC}_{\text{ref}}(k-1))/T_h/\Delta t$$
$$\text{SOC}_{\text{ref}}^{\text{end}} = \begin{cases} \text{SOC}_{\max}, & 500 \le T_d \le 600, \\ \text{SOC}_{\max}, & 300 \le T_d < 500 \\ \text{SOC}_{\min}, & 150 \le T_d < 300 \end{cases}$$
$$\text{SOC}_{\min} \le \text{SOC}_{\text{ref}}(k) \le \text{SOC}_{\max} \tag{8}$$

where $\text{SOC}_{\text{ref}}(k-1)$ —SOC reference at the last moment, $\text{SOC}_{\text{ref}}(k)$—current SOC reference, k_1—SOC_{ref} change slope, Δt —SOC_{ref} update time and $\text{SOC}_{\text{ref}}^{\text{end}}$—expected final value at the current departure interval.

During the actual operation, in order to prevent the battery from overcharging and overdischarging, the working range of the battery SOC is often limited. The working principle of the SOC limiting module is shown in Fig. 14. Where $\text{SOC}_{\min}$ is the lower limit of the battery SOC, $\text{SOC}_{\max}$ is the upper limit of the battery SOC, P_{ref} is the charging and discharging power demand of the ESS, $P_{\text{batt-ref}}$ is the charging and discharging power command value of ESS. When $\text{SOC} \ge \text{SOC}_{\max}$, the ESS is prohibited from charging; when $\text{SOC} \le \text{SOC}_{\min}$, the ESS is prohibited from discharging; when $\text{SOC}_{\min} < \text{SOC} < \text{SOC}_{\max}$, the ESS is working normally. In order to prevent SOC_{ref} from affecting

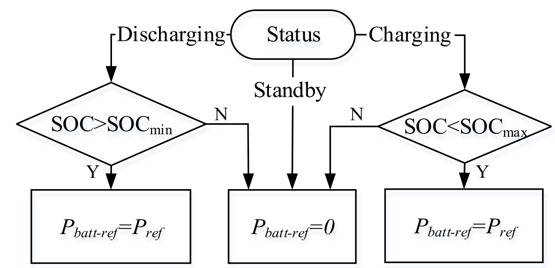

Fig. 14. SOC limit module working principle.

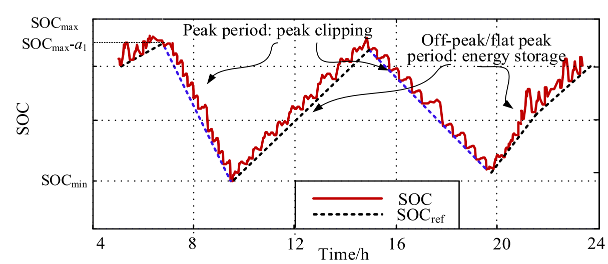

Fig. 15. The SOC_{ref} and SOC of the battery under the energy transfer strategy.

the recovery of the remaining regenerative braking energy, the working range of SOC_{ref} is limited from $\text{SOC}_{\min}$ to $\text{SOC}_{\max}$, which is smaller than the actual SOC operating range.

The changing slope k_1 is updated in real time according to $\text{SOC}_{\text{ref}}(\text{k}-1)$, $\text{SOC}_{\text{ref}}^{\text{end}}$ and the remaining duration T_h of the current departure interval, so as to avoid the influence of the initial value of SOC_{ref} in one day or the adjustment of the departure interval on energy transfer. In the off-peak period (500~600s) and flat peak period (300~500s), $\text{SOC}_{\text{ref}}^{\text{end}} = \text{SOC}_{\max}$, the BESS is guaranteed to store as much energy as possible at the end of the off-peak/flat peak period. In the peak period(150~300s), $\text{SOC}_{\text{ref}}^{\text{end}} = \text{SOC}_{\min}$, so that at the end of the peak period, $\text{SOC}_{\text{ref}} = \text{SOC}_{\min}$, the energy stored in the battery is effectively released. At different departure intervals k_1 is different, during the peak period, $k_1 < 0$, SOC_{ref} decreases; at the off-peak/flat peak period, $k_1 > 0$, SOC_{ref} increases, as shown in Fig. 15.

If $k_1 = 0$, then SOC_{ref} is kept constant, which is the existing control strategy, and the SOC of the ESS is maintained within a relatively small range.

B. Discharge Threshold Dynamic Adjustment Module

The discharge threshold dynamic adjustment module dynamically adjusts the discharge threshold based on the difference

TABLE III
ESS PARAMETERS

Parameters	Values	Parameters	Values
Rated voltage /V	500	Rated power /kW	2000
Rated current /A	4000	Total energy /kWh	590

ΔSOC between the battery SOC and SOC_{ref}, as shown in Equation (9). Where, ΔU_{dis} is the undetermined parameter, which is related to the train departure interval. U_{dis0} is the initial value of the discharge threshold, which changes with the fluctuation of no-load voltage and the departure interval. a_1, a_2, k_2 are all undetermined parameters, and a_1 is the judgment threshold of ΔSOC, a_2 is the decreasing value between U_{dis} and U_{sub}, k_2 is decreasing slope of the discharge threshold.

$$\begin{cases} U_{dis}(k) = \begin{cases} U_{dis0}, & \Delta\text{SOC} > a_1 \\ U_{dis0} - k_2/\Delta\text{SOC}(k), & 0 < \Delta\text{SOC} \le a_1 \\ U_{\text{sub}} - a_2, & \Delta\text{SOC} \le 0 \end{cases} \\ U_{dis0} = U_{d0} - \Delta U_{dis} \\ \Delta\text{SOC}(k) = \text{SOC}(k) - \text{SOC}_{\text{ref}}(k) \\ k_2 \ge 0, \text{SOC}_{\text{min}} \le \text{SOC}_{\text{ref}}(k) \le \text{SOC}_{\text{max}} \end{cases} \tag{9}$$

When $\Delta\text{SOC} > a_2$, the discharge threshold remains constant, $U_{\text{dis}} = U_{\text{dis0}}$. When $0 < \triangle$ SOC $\le a_2$, U_{dis} is dynamically adjusted according to the discharge thresholds U_{dis0} and ΔSOC, ($U_{\text{dis}} \le U_{\text{dis0}}$). As the ΔSOC decreases, the discharge threshold U_{dis} decreases, and the output power of the ESS is gradually reduced. When $\Delta\text{SOC} \le 0$, making $U_{\text{dis}} < U_{\text{sub}}$, the ESS exits the work, and the discharge threshold U_{dis} is adjusted to limit the discharge amount E_d of the ESS, so that the SOC can dynamically track SOC_{ref}, as shown in Fig. 15.

Under the above control strategy, the energy flow relationship of the ESS is shown in Equation (10) during the off-peak/flat peak period. Part of the energy E_c recovered by the ESS is stored in the ESS (E_s), part of the energy is lost in the impedance of the ESS and the converter (E_{loss}), and the rest is used for train traction (E_d). During the peak period, the energy flow relationship of the ESS is shown in Equation (11). The en-ergy used for the train traction is equal to the energy recovered by the ESS (E_c) and the stored energy of the ESS (E_s) minus the ESS loss (E_{loss}). In existing control strategies, E_s is 0.

$$E_d = E_c - E_s - E_{\text{loss}} \tag{10}$$

$$E_d = E_c + E_s - E_{\text{loss}} \tag{11}$$

V. SIMULATION ANALYSIS

Based on the simulation platform constructed above, the T-SOC control strategy is verified by simulation. This paper only considers a single ESS and places it in Substation 3. The parameters of the ESS are shown in Table III, rated power is 2 MW, and total energy is 590 kWh. The simulation parameters under the improved control strategy are shown in Table IV. Where the battery SOC is used in the range of 0.3∼0.9, and the SOC_{ref} range is 0.3∼0.8. Therefore, approximately 295 kWh (590 kWh × (0.8 − 0.3) = 295 kWh) of energy can be transferred from the off-peak/flat peak period to the peak period, which is transferred twice a day, and a total of 590 kWh of energy can be transferred. The charging threshold U_{char} of the ESS is 850 V. The initial discharge thresholds at different departure intervals are: 799.32 V (600s), 795.33 V (450s), 771.26 V (300s), 735.5 V (150s).

TABLE IV
IMPROVE CONTROL STRATEGY PARAMETERS

Parameters	Values	Parameters	Values
$SOC_{\min}$	0.3	$SOC_{\max}$	0.9
$\Delta t/s$	1	a_1	0.1
a_2	5		

TABLE V
SLOPE OF SOC_{ref} CHANGE AT DIFFERENT TIMES

Time	Departure interval	k_1	SOC_{ref} initial value	$SOC_{\text{ref}}^{\text{end}}$
20:30~23:30 5:30~6:30	300~600s	3.47*e-5	0.3	0.8
6:30~10:00	150~300s	-3.97*e-5	0.8	0.3
10:00~16:30	300~500s	1.98*e-5	0.3	0.8
16:30~20:30	150~300s	-3.47*e-5	0.8	0.3

Taking the departure interval shown in Fig. 7 as an example, the slope of SOC_{ref} change at different times is shown in Table V. 5:30∼6:00 and the previous day 20:30∼23:30, both periods are at off-peak/flat peak and need to be considered compreh-ensively. Take the early morning peak as an example, the duration is 3.5 h. Assuming that at the end of the early off-peak SOC_{ref} increases to 0.8, and peak period SOC_{ref} decreases from 0.8 to 0.3, so $k_1 = (0.3 - 0.8)/(3.5 \times 3600\text{s}) = -3.97\text{e-}5$. If SOC_{ref} does not reach 0.8 before the morning peak arrives, k_1 will be adjusted according to the current actual SOC_{ref} and duration T_h. Similarly, the slope of change k_1 for each time period can be obtained.

According to the parameter simulation determined in the previous section, the curve of the SOC and the curve of the discharge threshold U_{dis} of the ESS is shown in Fig. 16. In the off-peak /flat peak period, take the 600s/450s departure interval as an example, SOC_{ref} gradually increases with a certain slope, as show in Fig. 16 (a), (c). The discharge threshold is adjusted in real time to limit the discharge energy of the ESS, as show in Fig. 16(b), (d). The energy recovered by the ESS is greater than the released energy, and the rest is stored in the battery, so the battery SOC gradually increases to track SOC_{ref} dynamically. In the peak period, take the 300s/150s departure interval as an example, the SOC_{ref} gradually decreases, as show in Fig. 16(e), (g). And the energy stored in the battery is gradually released, which increases the discharge energy of the ESS during peak period. Energy transfer is realized without affecting the energy saving effect of the ESS.

Comparing the T-SOC strategy with the V-SOC strategy, the charging energy E_c, discharge energy E_d and peak power of the ESS under different strategies are shown in Table VI (single departure interval). As seen from the table, the peak power has

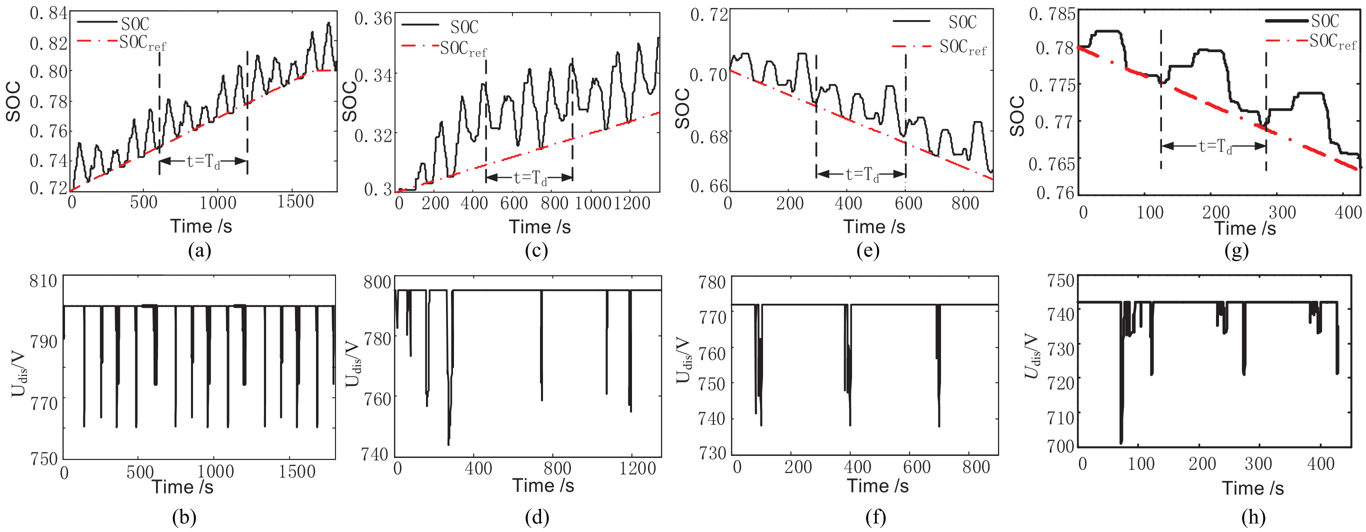

Fig. 16. SOC and U_{dis} of ESS under different departure intervals in T-SOC strategy. (a) $T_d = 600$ s, SOC curve. (b) $T_d = 600$ s, U_{dis} curve. (c) $T_d = 450$ s, SOC curve. (d) $T_d = 450$ s, U_{dis} curve. (e) $T_d = 300$ s, SOC curve. (f) $T_d = 300$ s, U_{dis} curve. (g) $T_d = 150$ s, SOC curve. (h) $T_d = 150$ s, U_{dis} curve.

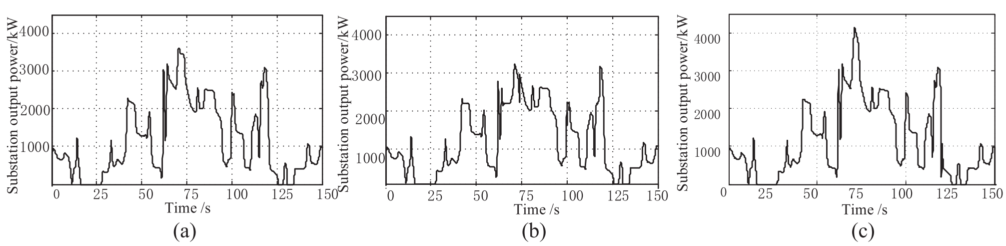

Fig. 17. Comparison of substation output under different working condition. (a) V-SOC strategy. (b) T-SOC strategy. (c) No ESS.

TABLE VI
COMPARISON BETWEEN V-SOC STRATEGIES AND T-SOC STRATEGIES

T_d/s		E_c/kWh	E_d/kWh	Peak power /kW
V-SOC	150	3.47	3.39	3620
	300	40.25	38.82	2092
	450	146.15	140.32	1283
	600	124.23	120.64	1322
T-SOC	150	3.47	6.87	3030
	300	40.25	42.33	1924
	450	146.15	127.42	1339
	600	124.23	103.44	1455

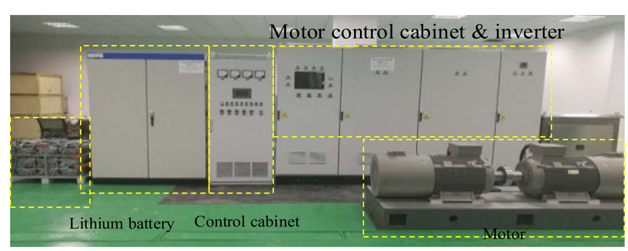

Fig. 18. Experimental platform structure.

been effectively reduced due to the increased energy released during the peak period. As seen from the table, under the control of the T-SOC strategy, in the off-peak period, $E_d > E_c$, in the peak period, $E_d > E_c$, the braking energy transfering from the off-peak period to the peak period is well realized. The peak power is reduced at the peak period, which in turn reduces the total peak power of the substation. Taking $T_d = 150$s as an example, compared with the existing control strategy, the discharge time and discharge power of the ESS are increased, the peak power is reduced by 590 kW, and the improvement rate is about 16.3%, so the substation capacity will be significantly reduced. Compared with no energy storage system, the peak power is reduced by 1110 kW, as shown in Fig. 17. Compared with the V-SOC strategy, the peak power of the substation increases slightly due to the decrease of the discharge energy E_d of the off-peak period and the flat peak period, but the design capacity of the traction substation is mainly determined by the peak power during peak period, so a slight increase in the off-peak period does not affect the effect.

VI. EXPERIMENTAL VERIFICATION

In order to verify the effectiveness of the dynamic thresholding control strategy based on the energy transfer threshold proposed in this paper, the experimental verification was carried out on the test platform of the 90 kW wayside BESS. The experimental platform simulates the actual construction of the urban rail power supply system as shown in Fig. 18.

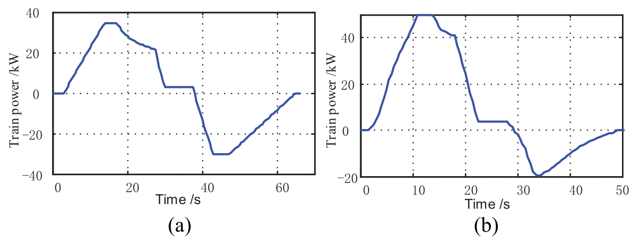

Fig. 19. The running power of the motor. (a) Condition (Off-peak). (b) Condition 2 (Peak).

TABLE VII
STATISTICS OF DIFFERENT WORKING CONDITIONS

	Max traction power/kW	Max braking power /kW	Traction energy /Wh	Braking energy /Wh
Case 1	34.6	28	172.6	117.5
Case 2	49.8	19.6	189.2	49.8

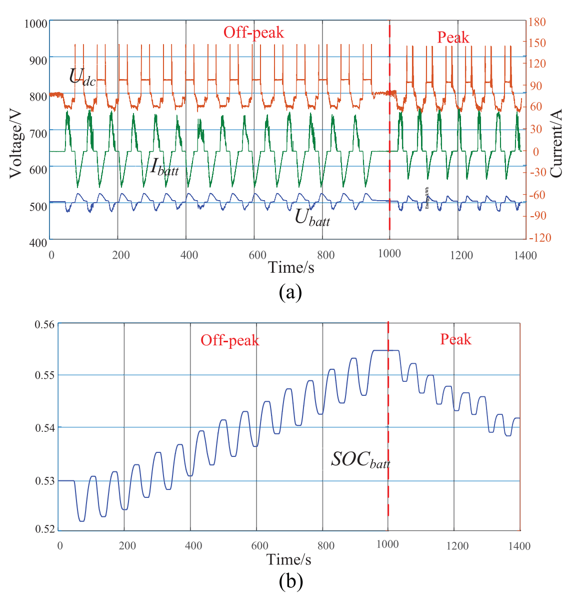

Fig. 20. Experimental result of improved control strategy. (a) Voltage and current waveforms. (b) SOC waveform.

This paper designs two operating conditions of the motor, as shown in Fig. 19. In condition 1, the traction power of the train is slightly smaller, the braking energy is more, the operation of the urban rail transit in the off-peak period is simulated and the ESS works in the energy storage mode. Under condition 2, the traction power of the train is larger and the braking energy is less. The operation of the urban rail transit is simulated during the peak period, and the ESS works in the peak clipping mode. The statistics of data under two operating conditions are shown in Table VII.

The experimental waveforms under different conditions are shown in Fig. 20. The SOC curve of the battery is estimated based on the charge and discharge currents of the battery. From the figure, we can see that in the off-peak conditions, the ESS charging current is greater than the discharge current, the battery's SOC

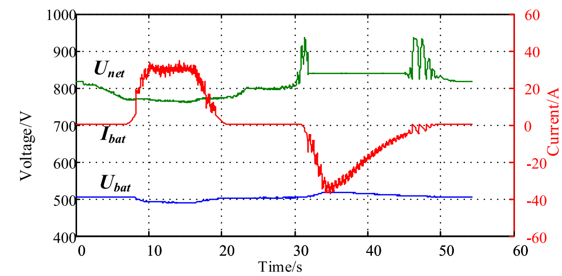

Fig. 21. Experimental result of V-SOC strategy.

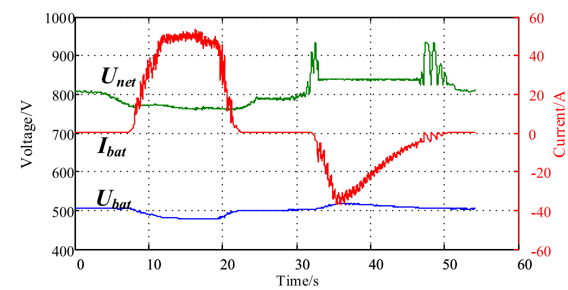

Fig. 22. Experimental result of T-SOC strategy.

TABLE VIII
ENERGY FLOWS AT DIFFERENT CONTROL STRATEGY

	E_{sub} output /Wh	ESS recover/Wh	ESS freed/Wh	U_{sub} max drop /V	P_{sub} peak /kW
V-SOC	150.3	44.82	42.579	55	31.1
T-SOC	129.7	44.82	60.21	47	26.4

increases by adjusting the discharge threshold. In peak operating conditions, the ESS discharge current is greater than the charging current, the SOC of the battery decreases dynamically.

In peak operating conditions, the experimental results of the train uses different control strategies in a traction braking cycle are shown in the Fig. (21), (22). Table VIII summarizes the energy flow under different control strategies in a traction and braking cycle. Under this control strategy, the battery stores some of the recovered energy during the off-peak period, shifts to the peak period, and gradually releases during the peak period, so that the discharge energy of the energy storage system is increased, the output of the substation is reduced, the drop of the network pressure is suppressed, and the peak power of the substation is reduced by 4.7% compared with V-SOC, significantly reduce the construction capacity and cost of the substation.

VII. CONCLUSION

In this paper, the load characteristics of urban rail transit with different departure intervals was analyzed by means of a dc traction power system model. Combined with the high energy density characteristic of the battery and the characteristic of the train running load. The SOC dynamic adjustment module and the discharge threshold dynamic adjustment module are added to dynamically adjust the discharge threshold. The energy transfer is realized without changing the energy saving effect, thereby reducing the peak power of the traction substation. According to the actual operation data of Beijing Batong Subway Line, the simulation and experiment were carried out. In the case study, by using the T-SOC strategy, the peak power was reduced by 590 kW and the improvement rate was 16.3% for the 2 MW BESS compared to the V-SOC strategy. In the 90 kW experiment, the substation peak power was reduced by 4.7 kW. It is thus proven that the energy management strategy of this paper can make full use of BESS to reduce the peak power of the substation and bring more benefits.

References

[1] H. Hayashiya *et al.*, "Recent trend of regenerative energy utilization in traction power supply system in Japan," *Urban Rail Transit*, vol. 3, no. 4, pp. 1–9, 2017.

[2] T. Ratniyomchai, S. Hillmansen, and P. Tricoli, "Recent developments and applications of energy storage devices in electrified railways," *IET Elect. Syst. Transp.*, vol. 4, no. 1, pp. 9–20, Mar. 2014.

[3] S. Khayyam, N. Berr, L. Razik, M. Fleck, F. Ponci, and A. Monti, "Railway system energy management optimization demonstrated at offline and online case studies," *IEEE Trans. Intell. Transp. Syst.*, vol. 19, no. 11, pp. 3570–3583, Nov. 2018.

[4] F. Ciccarelli, D. Iannuzzi, and I. Spina, "Comparison of energy management control strategy based on wayside ESS for LRV application," in *Proc. 39th Annu. Conf. IEEE Ind. Electron. Soc.*, Vienna, 2013, pp. 1548–1554.

[5] H. Hayashiya *et al.*, "Lithium-ion battery installation in traction power supply system for regenerative energy utilization: Initial report of effect evaluation after half a year operation," in *Proc. 16th Int. Power Electron. Motion Control Conf. Expo.*, Antalya, 2014, pp. 119–124.

[6] J. Hu, M. R. Sarker, J. Wang, F. Wen, and W. Liu, "Provision of flexible ramping product by battery energy storage in day-ahead energy and reserve markets," *IET Gener., Transmiss. Distribution*, vol. 12, no. 10, pp. 2256–2264, May 29, 2018.

[7] L. Qi *et al.*, "Comprehensive evaluation of hierarchical storage system based on analytic hierarchy process and improved technique for order preference by similarity to ideal solution," *Power Syst. Protection Control*, vol. 45, no. 3, pp. 13–19, 2017.

[8] T. Suzuki, H. Hayashiya, T. Yamanoi, and K. Kawahara, "Application examples of energy saving measures in Japanese DC feeding system," in *Proc. Int. Power Electron. Conf.*, Hiroshima, 2014, pp. 1062–1067.

[9] H. Xia *et al.*, "Optimal energy management, location and size for, stationary energy storage system in a metro line based on genetic algorithm," *Energies*, vol. 8, no. 10, pp. 11618–11640, 2015.

[10] H. Hayashiya *et al.*, "Proposal of a novel control method of Li-ion battery system for regenerative energy utilization in traction power supply system," in *Proc. IEEE Int. Power Electron. Motion Control Conf.*, Varna, 2016, pp. 298–303.

[11] Y. Takashi, U. Shigeki, and N. Yoshiaki, *Field Test of Hybrid Power Supply System for DC Electric Railways*. Osaka, Japan: West Japan Railway Company, 2010.

[12] A. Gao, F. Zhang, Z. Fu, Z. Zhang, and H. Li, "The SOC estimation and simulation of power battery based on self-recurrent wavelet neural network," in *Proc. Chinese Autom. Congr.*, Jinan, 2017, pp. 4247–4252.

[13] H. Takahashi, N. Tabata, and H. Ikarashi, "Lithium ion battery application in traction power supply system," in *Proc. 16th Int. Power Electron. Motion Control Conf. Expo.*, Sep. 2014, pp. 979–984.

[14] M. Sadakiyo, N. Nagaoka, and A. Ametani, "An optimal operating point control of lithium-ion battery in a power compensator for DC railway system," in *Proc. 42nd Int. Universities Power Eng. Conf.*, Brighton, 2007, pp. 681–686.

[15] I. Azizi and H. Radjeai, "A new strategy for battery and supercapacitor energy management for an urban electric vehicle," *Elect. Eng.*, vol. 100, no. 2, pp. 667–676, 2018.

[16] Y. Zhang and Y. Wei Li, "Energy management strategy for supercapacitor in droop-controlled DC microgrid using virtual impedance," *IEEE Trans. Power Electron.*, vol. 32, no. 4, pp. 2704–2716, Apr. 2017.

[17] A. El Mejdoubi, H. Chaoui, H. Gualous, and J. Sabor, "Online parameter identification for supercapacitor state-of-health diagnosis for vehicular applications," *IEEE Trans. Power Electron.*, vol. 32, no. 12, pp. 9355–9363, Dec. 2017.

[18] Z. Yang, Z. Yang, H. Xia, and F. Lin, "Brake voltage following control of supercapacitor-based energy storage systems in metro considering train operation state," *IEEE Trans. Ind. Electron.*, vol. 65, no. 8, pp. 6751–6761, Aug. 2018.

[19] Z. P. Yang, Z. H. Yang, H. Xia, F. Lin, and F. Q. Zhu, "Supercapacitor state based control and optimization for multiple energy storage devices considering current balance in urban rail transit," *Energies*, vol. 10, no. 4, Apr. 2017, Art. no. 520(1–19).

[20] F. Zhu, Z. Yang, H. Xia, and F. Lin, "Hierarchical control and full-range dynamic performance optimization of the supercapacitor energy storage system in urban railway," *IEEE Trans. Ind. Electron.*, vol. 65, no. 8, pp. 6646–6656, Aug. 2018.

[21] O. Gomozov, J. P. F. Trovão, X. Kestelyn, and M. R. Dubois, "Adaptive energy management system based on a real-time model predictive control with nonuniform sampling time for multiple energy storage electric vehicle," *IEEE Trans. Veh. Technol.*, vol. 66, no. 7, pp. 5520–5530, Jul. 2017.

[22] S. Shili, A. Hijazi, A. Sari, X. Lin-Shi, and P. Venet, "Balancing circuit new control for supercapacitor storage system lifetime maximization," *IEEE Trans. Power Electron.*, vol. 32, no. 6, pp. 4939–4948, Jun. 2017.

[23] A. Rufer, D. Hotellier, and P. Barrade, "A supercapacitor-based energy storage substation for voltage compensation in weak transportation networks," *IEEE Trans. Power Del.*, vol. 19, no. 2, pp. 629–636, Apr. 2004.

[24] T. Guo, Z. Yang, F. Lin, and S. Xiong, "Optimization of peak load shifting control strategy for battery energy storage system used in urban rail transit," in *Proc. 43rd Ann. Conf. IEEE Ind. Electron. Soc.*, Beijing, 2017, pp. 3901–3906.

[25] Z. Yang, Z. Yang, F. Lin, and H. Xia, "Improved control strategy of energy storage system considering train operation states," in *Proc. IEEE 20th Int. Conf. Intell. Transp. Syst.*, Yokohama, 2017, pp. 1–6.

[26] D. Iannuzzi, E. Pagano, and P. Tricoli, "The use of energy storage systems for supporting the voltage needs of urban and suburban railway contact lines," *Energies*, vol. 6, no. 4, pp. 1802–1820, 2013.

[27] F. Lin, X. Li, Y. Zhao, and Z. Yang, "Control strategies with dynamic threshold adjustment for supercapacitor energy storage system considering the train and substation characteristics in urban rail transit," *Energies*, vol. 9, no. 4, Apr. 2016, Art. no. 257(1–18).

[28] P. Pozzobon, "Transient and steady-state short-circuit currents in rectifiers for DC traction supply," *IEEE Trans. Veh. Technol.*, vol. 47, no. 4, pp. 1390–1404, Nov. 1998.

[29] J. Wang *et al.*, "Thresholds modification strategy of wayside supercapacitor storage considering DC substation characteristics," in *Proc. 41st Annu. Conf. IEEE Ind. Electron. Soc.*, Yokohama, 2015, pp. 002076–002081.

[30] Z. Yang, Z. Yang, X. Li, and F. Lin, "The real-time optimization of charge-/discharge voltage threshold for energy storage system in urban rail transit," in *Proc. 43rd Ann. Conf. IEEE Ind. Electron. Soc.*, Beijing, 2017, pp. 3930–3935.

[31] P. J. Grbović, P. Delarue, and P. Le Moigne, "Modeling and control of ultracapacitor based energy storage and power conversion system," in *Proc. IEEE 15th Workshop Control and Model. Power Electron.*, Santander, 2014, pp. 1–9.

Qiangqiang Qin (S'18) received the B.S. degree in electrical engineering in 2017 from Beijing Jiaotong University, Beijing, China, where he is currently working toward the master's degree at the School of Electrical Engineering. His research interests include energy management strategies of energy storage systems, energy-efficient models, and optimal operation of multiple trains in urban rail transit.

Tingting Guo (S'16) received the B.S. degree in electrical engineering from Beijing Jiaotong University, Beijing, China, in 2015. She is currently working with Beijing Hyperstrong Technology Co., Ltd. Her research interests include energy management strategies of energy storage systems, energy-efficient models, and optimal operation of multiple trains in urban rail transit.

Fei Lin (M'05) received the B.S. degree from Xi'an Jiaotong University, Xi'an, China, the M.S. degree from Shandong University, Jinan, China, and the Ph.D. degree from Tsinghua University, Beijing, China, in 1997, 2000, and 2004, respectively, all in electrical engineering. He is currently a Professor with the School of Electrical Engineering, Beijing Jiaotong University. His research interests include traction converters and motor drives, energy management for railway systems, and digital control of power-electronic-based devices.

Zhongping Yang (M'14) received the B.Eng.degree from the Tokyo University of Mercantile Marine, Tokyo, Japan, in 1997 and the M.Eng. and Ph.D. degrees from the University of Tokyo, Tokyo, Japan, in 1999 and 2002, respectively, all in electrical engineering. He is currently a Professor with the School of Electrical Engineering, Beijing Jiaotong University, Beijing, China. His research interests include high-speed rail integration technology, traction and regenerative braking technology, and wireless power transfer of urban rail vehicles. Prof. Yang received the Zhan Tianyou Award for Science and Technology in 2010, the Excellent Popular Science and Technology Book Award in 2011, and the Science and Technology Progress Award (second prize) of Ministry of Education in China in 2016.